

## Electron Coulomb effects in quasielastic ( $e, e'p$ ) reactions

Yanhe Jin, D. S. Onley, and L. E. Wright

*Physics Department, Ohio University, Athens, Ohio 45701*

(Received 14 October 1991)

We describe a calculation for the electron Coulomb distortion effects in ( $e, e'p$ ) in the quasielastic region from medium and heavy nuclei. The bound nucleons are described by single-particle Dirac wave functions in the presence of scalar and vector potentials which are parametrized fits to relativistic Hartree potentials, while the wave function of the knocked-out nucleon is a solution to the Dirac equation with the relativistic optical potential. The electron wave functions are solutions to the Dirac equation in the presence of the Coulomb potential of the nucleus and the interaction with the selected nucleon is treated to first order. We examine the  $^{40}\text{Ca}(e, e'p)$  reaction in both parallel and  $\omega$ - $q$  constant kinematics. We find that electron Coulomb distortion has a smaller effect in  $\omega$ - $q$  constant kinematics than in parallel kinematics. The principal effect in parallel kinematics is to shift the maximum and minimum of the reduced cross section which is consistent with the experimental data. Occupation numbers of about 70% to 80% are needed to normalize the distorted-wave Born approximation calculation to the  $^{40}\text{Ca}(e, e'p)$  experimental data. We also calculate the reduced cross section for the  $3s_{1/2}$  state in  $^{208}\text{Pb}$  and compare our results to experimental data and previous calculations. We find no significant difference in using relativistic, as compared with nonrelativistic, nuclear wave functions. We do find significant corrections to earlier methods of treating Coulomb distortion which, in turn, affect the occupation number extracted from experiment. We find an occupation number for this state of 71.4%.

PACS number(s): 25.30.-c, 24.90.+d

### I. INTRODUCTION

Analysis of ( $e, e'p$ ) reactions in the quasielastic region holds out the possibility of extracting single-particle wave functions and spectroscopic factors [1], at least within the independent particle shell model (IPSM). For  $^{40}\text{Ca}$ , theoretical models generally predict occupations of around 80% for levels just below the Fermi level [2,3]. Spectroscopic factors deduced experimentally from pickup reactions generally agree with the theoretical estimates [4,5]. However, analyses of the ( $e, e'p$ ) reaction on  $^{40}\text{Ca}$  have found spectroscopic factors of the order of 40–60% for valence protons [6]. These puzzling results were based on one or the other of two previous methods of analysis which differ in the way they include Coulomb distortions effects. One of these approaches uses an eikonal approximation to approximate the Coulomb distortion effects [7], while the other also used the same general approach we are using, but some approximations were made in treating the Coulomb distortion [8]. We also note that the eikonal-based calculations used nonrelativistic bound-state and continuum proton wave functions, while Ref. [8] used relativistic bound-state and continuum proton wave functions.

Using various techniques for handling electron Coulomb distortion that we have developed over the years [9], we have completed an analysis of ( $e, e'$ ) and ( $e, e'p$ ) which has removed all significant approximations which involve Coulomb distortions [10]. In this paper we report our investigations of the ( $e, e'p$ ) reactions from medium and heavy nuclei. In Sec. II we give the formalism for ( $e, e'p$ ) in the distorted-wave Born approximation (DWBA) and discuss our treatment of the bound and out-

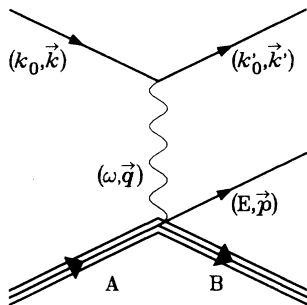
going proton wave functions. In Sec. III we relate our calculations to the commonly used reduced form  $\rho_m$  expressed as a function of “missing momentum”  $p_m$ ; we are then able to compare our calculations on  $^{40}\text{Ca}$  to experimental data from NIKHEF. We estimate the occupation numbers for two orbitals in  $^{40}\text{Ca}$  and find values closer to those given by theory and by other reactions. In Sec. IV we investigate ( $e, e'p$ ) from  $^{208}\text{Pb}$  and compare our calculations for the  $3s_{1/2}$  knockout to the experimental data from NIKHEF and to previous calculations. We extract the occupation number for this orbital. Finally, in Sec. V we give our conclusions.

### II. FORMALISM FOR INELASTIC ELECTRON SCATTERING

#### A. Kinematics and assumptions for the ( $e, e'p$ ) process

We choose to work in the laboratory frame of reference in which the target nucleus is at the origin of the coordinate system. As shown in Fig. 1, the incoming electron with four-momentum  $k_\mu = (k_0, \mathbf{k})$  defines the  $\hat{z}$  direction; the scattered electron with  $k'_\mu = (k'_0, \mathbf{k}')$  is moving in the  $x$ - $z$  plane ( $\phi_e = 0$ ). The ejected proton has  $p_\mu = (E, \mathbf{p})$  with its direction described by the polar angles  $(\theta_p, \phi_p)$ . We use  $q_\mu = (\omega, \mathbf{q})$  to denote the four-momentum transfer. Throughout we use units such that ( $\hbar = c = 1$ ).

In our calculations we make the following assumptions: (1) The incoming and outgoing electrons are described by wave functions distorted by the nuclear Coulomb potential. (2) The virtual photon emitted by the electron is absorbed by a single nucleon. All other nu-

FIG. 1. Kinematics for the  $(e, e'p)$  process.

cleons are just spectators in the process. (3) The ejected nucleon interacts with the residual nucleus through a relativistic optical potential. (4) The bound nucleon is described by an independent particle model in a relativistic Hartree potential. With these conditions satisfied, we will refer to the calculation as the distorted-wave Born approximation (DWBA). Where we ignore the Coulomb distortion (the first condition) and use plane waves to describe the electrons, we will label the calculation plane-wave Born approximation (PWBA), despite the fact that the outgoing nucleon is still a distorted wave. If we ignore the nucleon final-state interaction, we say explicitly that we are using a plane wave for the nucleon.

The distorted-wave functions for the electrons are obtained by numerically solving the Dirac equation in the presence of the static Coulomb potential of the nuclear charge distribution. Thus the Coulomb distortion of the electron waves from the static Coulomb field of the nucleus is included to all orders. The Coulomb distorted incoming electron wave function can be written as a sum of partial waves,

$$\Psi_{\text{in}}(\mathbf{r}) = \sum_{\kappa\mu} C_{\kappa\mu} \exp(i\delta_{\kappa}) \psi_{\kappa\mu}(\mathbf{r}), \quad (1)$$

where  $\psi_{\kappa,\mu}$  is the electron eigenstate with angular momentum quantum number  $\kappa, \mu$  given explicitly by

$$\psi_{\kappa\mu}(\mathbf{r}) = \begin{bmatrix} f_{\kappa}(r) \mathcal{Y}_{\kappa,\mu}(\hat{\mathbf{r}}) \\ ig_{\kappa}(r) \mathcal{Y}_{-\kappa,\mu}(\hat{\mathbf{r}}) \end{bmatrix}, \quad (2)$$

and the spin angle functions are

$$\mathcal{Y}_{\kappa,\mu}(\hat{\mathbf{r}}) = \sum_s \langle l\mu - s \frac{1}{2}s | j\mu \rangle Y_{l\mu-s}(\hat{\mathbf{r}}). \quad (3)$$

To satisfy the incoming boundary condition, we need

$$C_{\kappa\mu} = \left[ \frac{k_0 + m}{2k_0} \right]^{1/2} \langle l\mu - s \frac{1}{2}s | j\mu \rangle i^l Y_{l\mu-s}(\hat{\mathbf{k}}), \quad (4)$$

and  $\delta_{\kappa}$  is the phase shift for the  $\kappa$  partial wave,  $m$  is the electron mass, and  $s$  is the electron-spin projection. For the outgoing electron,

$$\Psi_{\text{out}}(\mathbf{r}) = \sum_{\kappa'\mu'} C_{\kappa'\mu'} \exp(-i\delta_{\kappa}') \psi_{\kappa'\mu'}(\mathbf{r}). \quad (5)$$

We use global optical potentials [1], obtained from fitting elastic proton-scattering data, to describe the proton

final-state interaction. The wave function for the outgoing proton has the same structure as that for the outgoing electron:

$$\Psi_p(\mathbf{r}) = \sum_{\kappa_p\mu_p} C_{\kappa_p\mu_p} \exp(-i\delta_{\kappa_p}^*) \begin{bmatrix} f_{\kappa_p}^*(r) \mathcal{Y}_{\kappa_p,\mu_p}(\hat{\mathbf{r}}) \\ ig_{\kappa_p}^*(r) \mathcal{Y}_{-\kappa_p,\mu_p}(\hat{\mathbf{r}}) \end{bmatrix}, \quad (6)$$

where  $C_{\kappa_p\mu_p}$  and  $\mathcal{Y}_{\kappa_p,\mu_p}(\hat{\mathbf{r}})$  are defined as in Eqs. (3) and (4) with the proton energy, mass, angular momentum, etc., replacing the electron values. Since  $f$  and  $g$  are the solutions of the Dirac equation with complex potentials and must satisfy incoming boundary conditions, we must use  $f^*$  and  $g^*$  and  $\delta_{\kappa_p}^*$  for the wave function to describe the outgoing channel.

Finally, the bound-state wave function can be written in terms of the Dirac quantum numbers  $\kappa_b$  and  $\mu_b$ :

$$\psi_{\kappa_b\mu_b}(\mathbf{r}) = \left[ \frac{E_b + m_N}{2E_b} \right]^{1/2} \begin{bmatrix} f_{\kappa_b}(r) \mathcal{Y}_{\kappa_b,\mu_b}(\hat{\mathbf{r}}) \\ ig_{\kappa_b}(r) \mathcal{Y}_{-\kappa_b,\mu_b}(\hat{\mathbf{r}}) \end{bmatrix}, \quad (7)$$

where  $m_N$  is the nucleon mass. All the radial functions given above satisfy the standard coupled first-order differential equations arising from the partial-wave decomposition of the Dirac equation with the appropriate vector and scalar potentials for the protons and with simply the Coulomb potential for the electrons.

## B. DWBA cross section

In electron-scattering calculations using the Born approximation, the main task is to evaluate the transition matrix elements. The interaction is well known from electrostatics:

$$H_i = - \int J^\mu A_\mu d\mathbf{r}, \quad (8)$$

where  $J^\mu$  is the nucleon transition current and  $A_\mu$  is the potential generated by the electron transition current  $j_\mu$ . In the Lorentz gauge the potential can be written in terms of the retarded Green function  $G(\mathbf{r}, \mathbf{r}') = \exp(i\omega|\mathbf{r}-\mathbf{r}'|)/|\mathbf{r}-\mathbf{r}'|$  as

$$A_\mu(\mathbf{r}) = \int j_\mu G(\mathbf{r}, \mathbf{r}') d\mathbf{r}'. \quad (9)$$

In the DWBA the nucleon and electron currents are complicated and the only way to evaluate the transition matrix elements is through partial-wave analysis. We can expand the scalar Green function in terms of the spherical harmonics, i.e.,

$$G(\mathbf{r}, \mathbf{r}') = 4\pi i \omega \sum_{LM} j_L(\omega r_<) h_L(\omega r_>) Y_{LM}(\hat{\mathbf{r}}) Y_{L,M}^*(\hat{\mathbf{r}}'), \quad (10)$$

where  $j_L$  denotes the spherical Bessel function and  $h_L$  denotes the spherical Hankel function of the first kind;  $r_>$  refers to whichever of  $\mathbf{r}$  and  $\mathbf{r}'$  has the larger magnitude and  $r_<$  to the one with the smaller magnitude. For the three-vector current terms, we can expand the Green function with the dyadic  $\bar{\mathbb{I}}$  in vector spherical harmonics  $\mathbf{Y}_{J,L}^M(\hat{\mathbf{r}})$  [12]:

$$\begin{aligned} \vec{G}(\mathbf{r}, \mathbf{r}') &= \vec{I}G(\mathbf{r}, \mathbf{r}') \\ &= 4\pi i \omega \sum_{JML} [j_L(\omega r_{<}) h_L(\omega r_{>}) \mathbf{Y}_{J,L}^{M*}(\hat{\mathbf{r}}) \mathbf{Y}_{J,L}^M(\hat{\mathbf{r}}')] . \end{aligned} \quad (11)$$

In terms of these expansions we can write the transition matrix element as

$$\begin{aligned} H_i &= -4\pi i \omega \sum_{LM} \left[ \int_0^\infty \rho^e Y_{LM}^*(\hat{\mathbf{r}}) \left( h_L(\omega r) \int_0^r \rho^N j_L(\omega r') Y_{LM}(\hat{\mathbf{r}}') d\mathbf{r}' + j_L(\omega r) \int_r^\infty \rho^N h_L(\omega r') Y_{LM}(\hat{\mathbf{r}}') d\mathbf{r}' \right) d\mathbf{r} \right. \\ &\quad \left. - \sum_J \int_0^\infty \mathbf{j} \cdot \mathbf{Y}_{LJ}^{M*}(\hat{\mathbf{r}}) \left( h_J(\omega r) \int_0^r \mathbf{J} \cdot \mathbf{Y}_{LJ}^M(\hat{\mathbf{r}}') j_J(\omega r') d\mathbf{r}' + j_J(\omega r) \int_r^\infty \mathbf{J} \cdot \mathbf{Y}_{LJ}^M(\hat{\mathbf{r}}') h_J(\omega r') d\mathbf{r}' \right) d\mathbf{r} \right] . \end{aligned} \quad (12)$$

The nucleon transition current will be the matrix element

$$J_\mu = \bar{\Psi}_p \hat{J}_\mu \psi_{\kappa_b \mu_b} , \quad (13)$$

where  $\hat{J}_\mu$  is the nucleon current operator. For a free nucleon the operator consists of two parts, namely, the Dirac contribution and the contribution of the anomalous magnetic moment  $\mu_T$ :

$$\hat{J}^\mu = F_1 \gamma^\mu + F_2 \frac{i\mu_T}{2m_N} \sigma^{\mu\nu} q_\nu . \quad (14)$$

When written separately the zero component (charge density) and three-vector current are

$$\hat{J}_0 = F_1 \gamma_0 + \frac{\mu_T}{2m_N} F_2 \boldsymbol{\alpha} \cdot \mathbf{q} , \quad (15)$$

$$\hat{\mathbf{J}} = F_1 \boldsymbol{\gamma} + F_2 \frac{\mu_T q_0}{2m_N} \boldsymbol{\alpha} + F_2 \frac{i\mu_T}{2m_N} \boldsymbol{\Sigma} \times \mathbf{q} . \quad (16)$$

Note here  $q_0 = \omega$  and  $\mathbf{q}$  is an operator in configuration space. The form factors  $F_1$  and  $F_2$  are related to the electric and magnetic form factors  $G_E$  and  $G_M$  by

$$G_E = F_1 + \frac{q_\mu^2 \mu_T}{4m_N^2} F_2 , \quad (17)$$

$$G_M = F_1 + \mu_T F_2 , \quad (18)$$

where  $q_\mu^2 = \omega^2 - q^2$  is the invariant square of the four momentum transfer. We will assume that  $G_E$  and  $G_M$  take the usual dipole form [13] for the proton:

$$G_E = G_M / (\mu_T + 1) = \frac{1}{(1 - q_\mu^2 / 0.71)^2} , \quad (19)$$

where in this formula  $q_\mu$  is in units of GeV. We evaluate these form factors at  $q_\mu^2$  given by the asymptotic electron energy and momentum, which amounts to an approximation, since, strictly speaking, our calculation requires that the point proton wave functions be convoluted with the proton charge and magnetization distributions in space. These are of course equal in electron plane-wave calculations, but not in DWBA calculations. However, with the values of energy and momentum transfer in experiments done to date, this approximation should make an insignificant difference. Using these definitions, we can work out the matrix element integrals given in Eq. (12). We find the following for the nucleon current operator matrix elements (details are given in Appendix D of Ref. [10]):

$$\begin{aligned} \int \bar{\psi}_{\kappa_p \mu_p} \hat{J}_0 \psi_{\kappa_b \mu_b} j_L(\omega r) Y_{LM}(\hat{\mathbf{r}}) d\Omega \\ = \langle j_b \mu_b LM | j_p \mu_p \rangle I_{\kappa_b \kappa_p}^L K_S^n \{r, j_L(\omega r)\} , \end{aligned} \quad (20)$$

where  $I_{\kappa_b \kappa_p}^L$  is the standard reduced spin-angle matrix element

$$I_{\kappa' \kappa} = \langle \mathcal{Y}_{\kappa', \mu'}(\hat{\mathbf{r}}) || Y_{LM} || \mathcal{Y}_{\kappa, \mu}(\hat{\mathbf{r}}) \rangle , \quad (21)$$

which is independent of the magnetic quantum numbers  $\mu, \mu', M$  and the signs of  $\kappa, \kappa'$ . It is understood that this matrix element is nonzero only when the angular momentum selection rule is followed: i.e.,  $l + l' + L = \text{even}$  for electric transition and  $\bar{l} + l' + L = \text{even}$  for magnetic transition. Note that  $l$  is the nonrelativistic orbital angular momentum determined by  $\kappa$ ,  $l(\kappa) = j + \text{sgn}(\kappa)$  ( $j$  being the corresponding total angular momentum), and  $\bar{l} = l(-\kappa)$ . The radial kernels  $K_S^n \{r, j_L(\omega r)\}$  can be written as

$$\begin{aligned} K_S^n \{r, j_L(\omega r)\} &= F_1 (f_{\kappa_p} f_{\kappa_b} + g_{\kappa_p} g_{\kappa_b}) j_L(\omega r) \\ &\quad + \frac{F_2 \mu_T \omega}{2m_N} \frac{1}{2L+1} \{ (f_{\kappa_p} g_{\kappa_b} + g_{\kappa_p} f_{\kappa_b}) [(L+1)j_{L+1}(\omega r) - Lj_{L-1}(\omega r)] \\ &\quad + (\kappa_p - \kappa_b) (f_{\kappa_p} g_{\kappa_b} - g_{\kappa_p} f_{\kappa_b}) [j_{L+1}(\omega r) + j_{L-1}(\omega r)] \} . \end{aligned} \quad (22)$$

For the vector part,

$$\int \bar{\psi}_{\kappa_p \mu_p} \hat{\mathbf{j}} \psi_{\kappa_b \mu_b} j_L(\omega r) \cdot \mathbf{Y}_{LJ}^M(\mathbf{r}) d\Omega = \langle j_b \mu_b LM | j_p \mu_p \rangle I_{\kappa_b \kappa_p} K_V^n \{r, j_J(\omega r)\}, \quad (23)$$

where  $J=L$ ,  $L \pm 1$ . The corresponding quantities  $K_V^n$  are written in terms of the proton wave functions in the following way:

$$\begin{aligned} K_V^n \{r, j_L(\omega r)\} = & \frac{-i}{\sqrt{L(L+1)}} \left\{ j_L(\omega r)(\kappa_p + \kappa_b) \left[ F_1(f_{\kappa_p} g_{\kappa_b} + g_{\kappa_p} f_{\kappa_b}) + \frac{F_2 \mu_T \omega}{2m_N} (f_{\kappa_p} g_{\kappa_b} - g_{\kappa_p} f_{\kappa_b}) \right] \right. \\ & + \frac{\mu_T \omega F_2}{2m_N 2L+1} \{ (\kappa_p + \kappa_b)(f_{\kappa_p} g_{\kappa_b} + g_{\kappa_p} f_{\kappa_b}) [L j_{L+1}(\omega r) - (L+1) j_{L-1}(\omega r)] \\ & \left. + L(L+1)(f_{\kappa_p} g_{\kappa_b} - g_{\kappa_p} f_{\kappa_b}) [j_{L+1}(\omega r) + j_{L-1}(\omega r)] \right\}, \quad (24) \end{aligned}$$

$$\begin{aligned} K_V^n \{r, j_{L-1}(\omega r)\} = & \frac{i}{\sqrt{L(2L+1)}} \left\{ j_{L-1}(\omega r) \left[ \left[ F_1(\kappa_p - \kappa_b) - L \frac{F_2 \mu_T \omega}{2m_N} \right] (f_{\kappa_p} g_{\kappa_b} + g_{\kappa_p} f_{\kappa_b}) \right. \right. \\ & + \left. \left[ (\kappa_p - \kappa_b) \frac{F_2 \mu_T \omega}{2m_N} - L F_1 \right] (f_{\kappa_p} g_{\kappa_b} - g_{\kappa_p} f_{\kappa_b}) \right] \\ & \left. + \frac{F_2 \mu_T \omega}{2m_N} (\kappa_p - \kappa_b) j_L(\omega r) (f_{\kappa_p} f_{\kappa_b} + g_{\kappa_p} g_{\kappa_b}) \right\}, \quad (25) \end{aligned}$$

$$\begin{aligned} K_V^n \{r, j_{L+1}(\omega r)\} = & \frac{i}{\sqrt{(L+1)(2L+1)}} \left\{ j_{L+1}(\omega r) \left[ \left[ F_1(\kappa_p - \kappa_b) + (L+1) \frac{F_2 \mu_T \omega}{2m_N} \right] (f_{\kappa_p} g_{\kappa_b} + g_{\kappa_p} f_{\kappa_b}) \right. \right. \\ & + \left. \left[ (\kappa_p - \kappa_b) \frac{F_2 \mu_T \omega}{2m_N} + F_1(L+1) \right] (f_{\kappa_p} g_{\kappa_b} - g_{\kappa_p} f_{\kappa_b}) \right] \\ & \left. - \frac{F_2 \mu_T \omega}{2m_N} (\kappa_p - \kappa_b) j_L(\omega r) (f_{\kappa_p} f_{\kappa_b} + g_{\kappa_p} g_{\kappa_b}) \right\}. \quad (26) \end{aligned}$$

In the above expressions, the spherical Bessel function  $j_L$  can be replaced by  $h_L$  when required [see Eq. (30)].

In the same way, we can work out the corresponding integrals for the electron part and define the corresponding  $K_S^e$  and  $K_V^e$ :

$$\int \bar{\psi}_{\kappa' \mu'} \hat{\mathbf{j}}_0 \psi_{\kappa \mu} j_L(\omega r) \cdot \mathbf{Y}_{LM}^*(\mathbf{r}) d\Omega = \langle j \mu L - M | j' \mu' \rangle I_{\kappa \kappa'} (-1)^M K_S^e \{r, j_L(\omega r)\} \quad (27)$$

and

$$\int \bar{\psi}_{\kappa \mu} \hat{\mathbf{j}} \psi_{\kappa' \mu'} j_J(\omega r) \cdot \mathbf{Y}_{LJ}^{M*}(\hat{\mathbf{r}}) d\Omega = \langle j \mu L - M | j' \mu' \rangle (-1)^{L+J+M+1} I_{\kappa \kappa'} K_V^e \{r, j_J(\omega r)\}. \quad (28)$$

Because the electron has no form factor and we neglect its anomalous magnetic moment, expressions for  $K_S^e$  and  $K_V^e$  can be obtained by replacing the proton mass and angular momenta in Eqs. (22)–(28) by the electron values and setting  $F_1=1$  and  $F_2=0$ . In terms of these integrals, we can write the transition matrix element

$$H_i = 4\pi i \omega \sum C_{\kappa \mu} C_{\kappa' \mu'}^* C_{\kappa_p \mu_p}^* (-1)^M \langle j_b \mu_b LM | j_p \mu_p \rangle \langle J \mu L - M | J' \mu' \rangle I_{|\kappa_b| |\kappa_p|} I_{|\kappa| |\kappa'|} R_{\kappa_b \kappa_p}^{\kappa \kappa'}(r), \quad (29)$$

where the summation is understood to run over  $\kappa \mu \kappa' \mu' \kappa_p \mu_p$  and  $LM$ . The complete radial integral,  $R_{\kappa_b \kappa_p}^{\kappa \kappa'}(r)$ , is given by

$$\begin{aligned}
R_{\kappa_b \kappa_p}^{\kappa \kappa'}(r) = & P_e \int_0^\infty \left[ K_S^e\{r, h_L(\omega r)\} \int_0^r K_S^n\{r', j_L(\omega r')\} r'^2 dr' \right. \\
& \left. + K_S^e\{r, j_L(\omega r)\} \int_r^\infty K_S^n\{r', h_L(\omega r')\} r'^2 dr' \right] r^2 dr \\
& - P_e \int_0^\infty \left[ K_V^e\{r, h_{L-1}(\omega r)\} \int_0^r K_V^n\{r', j_{L-1}(\omega r')\} r'^2 dr' \right. \\
& \left. + K_V^e\{r, j_{L-1}(\omega r)\} \int_r^\infty K_V^n\{r', h_{L-1}(\omega r')\} r'^2 dr' \right] r^2 dr \\
& - P_e \int_0^\infty \left[ K_V^e\{r, h_{L+1}(\omega r)\} \int_0^r K_V^n\{r', j_{L+1}(\omega r')\} r'^2 dr' \right. \\
& \left. + K_V^e\{r, j_{L+1}(\omega r)\} \int_r^\infty K_V^n\{r', h_{L+1}(\omega r')\} r'^2 dr' \right] r^2 dr \\
& + P_m \int_0^\infty \left[ K_V^e\{r, h_L(\omega r)\} \int_0^r K_V^n\{r', j_L(\omega r')\} r'^2 dr' \right. \\
& \left. + K_V^e\{r, j_L(\omega r)\} \int_r^\infty K_V^n\{r', h_L(\omega r')\} r'^2 dr' \right] r^2 dr, \tag{30}
\end{aligned}$$

where we have put in explicitly the factors for the angular momentum selection rule:  $P_e = 1$  means electric multipole conditions are satisfied, and  $P_m = 1$  for magnetic multipole. Explicitly,

$$P_e = \frac{1}{4} [1 + (-1)^{l+l'+L}] [1 + (-1)^{l_b+l_p+L}], \tag{31}$$

$$P_m = \frac{1}{4} [1 + (-1)^{\bar{l}+l'+L}] [1 + (-1)^{\bar{l}_b+l_p+L}]. \tag{32}$$

Finally, we write down the cross section in terms of the transition matrix element:

$$\frac{d^3\sigma}{d\Omega_e dk'_0 d\Omega_p} = \frac{k'_0 k_0 k'}{4\pi^2 k} \frac{1}{2} \sum_{\text{spin}} \frac{1}{2j_b + 1} \sum_{\mu_b \mu_p} |H_i|^2 \rho_p, \tag{33}$$

where  $\rho_p = pE / (2\pi)^3$  is the density of states for the ejected proton.

### III. COMPARISON WITH EXPERIMENTS

A popular way of presenting ( $e, e'p$ ) results is to calculate  $\rho_m$ , which for proton plane waves in the final state is directly related to the probability that a bound proton from a given shell with momentum  $\mathbf{p}_m$  can be knocked out of the nucleus. This can be related to the cross section in the plane-wave impulse approximation (PWIA) by

$$\rho_m(\mathbf{p}_m) = \frac{1}{pE \sigma_{ep}} \frac{d^3\sigma}{dk'_0 d\Omega_k d\Omega_p}, \tag{34}$$

where  $\mathbf{p}_m$  is called the missing momentum and can be determined by the kinematics  $\mathbf{p}_m = \mathbf{p} - \mathbf{q}$ . The off-shell electron-proton cross section  $\sigma_{ep}$  is not uniquely defined, but the commonly used expression is  $\sigma^{\text{cc1}}$  given by

De Forest [14]. In our calculations we adopt the same definition since the experimental data is usually presented in terms of  $\rho_m$ . We cannot, however, interpret the quantity in any simple way; in particular,  $\rho_m$  now depends on the electron kinematics.

Up to now, all the ( $e, e'p$ ) experiments have been carried out using one of two kinematic arrangements, called parallel kinematics and  $\omega$ - $q$  constant kinematics. In parallel kinematics one only observes protons ejected along the momentum-transfer direction  $\mathbf{q}$  and measures their energy spectrum. By varying the incoming and outgoing electron energies and the scattering angle, a variety of spectra for different momentum transfers is obtained. In  $\omega$ - $q$  constant kinematics, the energy and momentum transfer are fixed by fixing the electron kinematics and the proton angular distributions are measured. So far, only in-plane proton angular distributions have been measured.

#### A. Comparison to $^{40}\text{Ca}$ ( $e, e'p$ ) experimental data

As noted in the Introduction, we carry out the calculation in the laboratory frame (target fixed frame). Numerically, it takes less time to do a  $\omega$ - $q$  constant kinematics calculation than a parallel kinematics calculation because the radial integrals, which take much of the computational time, do not depend on the angles  $\theta_e$ ,  $\theta_p$ , etc., but depend on the incoming and outgoing electron energies; hence parallel kinematics requires they be recalculated for each point. So we prefer to study  $\omega$ - $q$  constant kinematic data. All of the data shown are from NIKHEF [6].

In Fig. 2 we show a calculation which corresponds to knocking out a proton from a  $2s_{1/2}$  orbit in  $^{40}\text{Ca}$ . The ki-

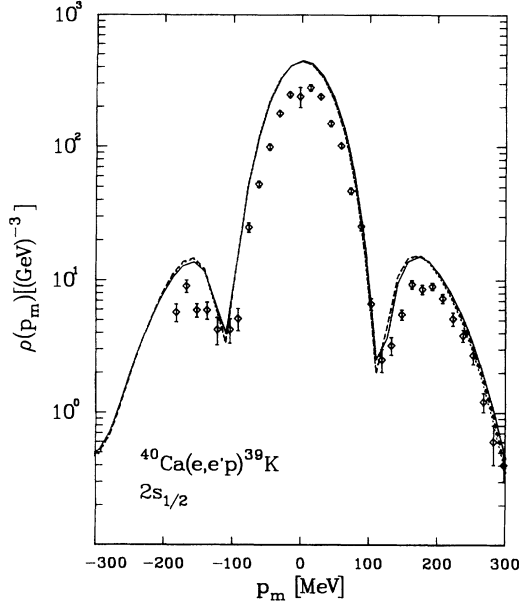


FIG. 2. Reduced cross section for  $^{40}\text{Ca}(e,e'p)^{39}\text{K}$  from the  $2s_{1/2}$  shell with  $\omega$ - $q$  constant kinematics. The kinematics are  $k_0=375$  MeV,  $k'_0=275$ , and  $p=q$ . The corresponding electron-scattering angle is  $\theta_e=83^\circ$ . The solid line is the DWBA calculation, the dashed line is the DWBA calculation with  $Z=1$ , and the dotted line the PWBA calculation.

nematics are  $k_0=375$  MeV,  $k'_0=275$ , and  $p=q$ , which means that at one proton angle we have the precise match  $q=p$ , which marks the top of the quasielastic peak; the corresponding electron-scattering angle is  $\theta_e=83^\circ$ . The solid line is our DWBA calculation; the dotted line is the PWBA calculation. The PWBA calculation should agree with the DWBA calculation in the limit  $Z\rightarrow 0$ ; our expressions become indeterminate in this limit, and hence in testing the program we choose an artificially small value of  $Z$  and compare with the PWBA. Therefore, in Fig. 2 we also show a dashed line, which is the DWBA calculation with  $Z=1$ . These results also show that the electron Coulomb distortions give no distinct contribution over the whole region shown; the peak in the middle stays roughly the same, and the two small ones are suppressed a little by the electron Coulomb distortion. Although we expect the electron Coulomb distortion effect due to the  $^{40}\text{Ca}$  target to be small, we did expect it to be somewhat larger. To understand this we varied the kinematic conditions to see if Coulomb distortion effects show up in other cases, for example, if we change the kinematics to move away from the quasielastic peak. Figures 3 and 4 show such calculations, where we chose the electron-scattering angle to be  $\theta_e=60^\circ$  and  $120^\circ$ , respectively ( $k'_0=265$  MeV). The horizontal straight lines are the regions of  $p_m$  which cannot be reached by the kinematics used. Compared with the PWBA calculation, note that the Coulomb distortion changes the amplitudes of the peaks, and also shifts the peaks, toward high  $p_m$  in Fig. 3, but toward low  $p_m$  in Fig. 4. In Fig. 3,  $\theta_e=60^\circ$ , which corresponds to  $q < p$ , and in Fig. 4,  $\theta_e=120^\circ$ , which corresponds to  $q > p$ , and

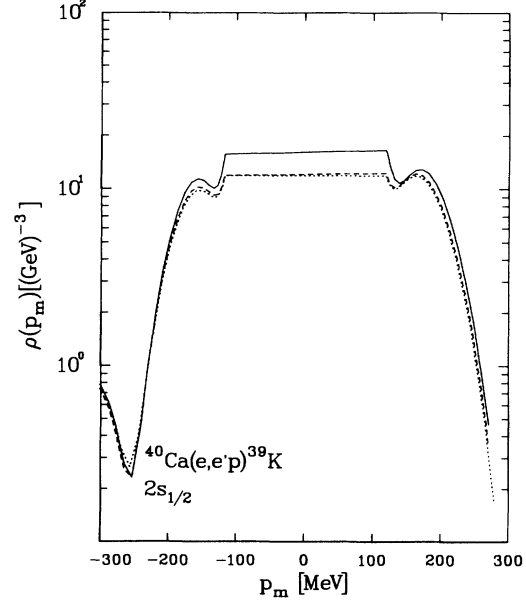


FIG. 3. Reduced cross section for  $^{40}\text{Ca}(e,e'p)^{39}\text{K}$  from the  $2s_{1/2}$  shell with off-peak  $\omega$ - $q$  constant kinematics. The kinematics are  $k_0=375$  MeV,  $k'_0=265$ , and  $p > q$ ;  $\theta_e=60^\circ$ . The solid line is the DWBA calculation, the dashed line is the DWBA calculation with  $Z=1$ , and the dotted line the PWBA calculation.

remembering  $p_m=p-q$ , we can see that in both cases Coulomb distortion shifts peaks toward lower  $q$ .

The jump from positive to negative values of  $p_m$  is an artifact of this kind of plot. For  $\omega$ - $q$  constant kinematics, the direction of the outgoing proton momentum is the significant variable. As it swings around, at some point  $p$

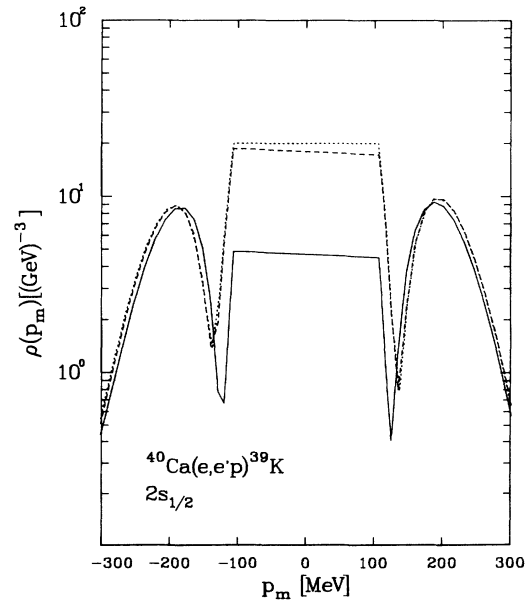


FIG. 4. Reduced cross section for  $^{40}\text{Ca}(e,e'p)^{39}\text{K}$  from the  $2s_{1/2}$  shell with off-peak  $\omega$ - $q$  constant kinematics. The kinematics are  $k_0=375$  MeV,  $k'_0=265$ , and  $p < q$ ;  $\theta_e=120^\circ$ . The solid line is the DWBA calculation, dashed line is the DWBA calculation with  $Z=1$ , and the dotted line the PWBA calculation.

passes  $q$ , at which point the missing momentum  $p_m$  ( $=p-q$ ) has a minimum magnitude  $|p-q|$  and also points along  $q$ . But  $p_m$  vectors to the right of  $q$  and to the left of  $q$  are not equivalent, although they may have the same magnitude. They are distinguished on the plot by sign,  $+|p_m|$  and  $-|p_m|$ : Values between  $\pm|p-q|$  are not physically accessible, and this region is bridged by a straight line. The points at either end of the straight lines should correspond to the same kinematics if we chose  $q \parallel p$ . However, in some figures,  $p$  is not exactly parallel to  $q$ . We know from the discussions above that peaks are shifted toward higher  $p_m$  for  $p < q$  and toward lower  $p_m$  for  $p > q$ , and hence we can anticipate the distortion effect in parallel kinematics; i.e., all DWBA peaks will shift to the right (increasing  $p_m$ ). In Fig. 5 we show the corresponding calculation in parallel kinematics. As expected, while leaving the point at  $p=q$  changed very little, the DWBA calculation shifts the curve to the right, so that the minimum shown by the experiment is well reproduced. Also, note that the electron distortions affect the  $p_m > 0$  and  $p_m < 0$  regions differently; the  $p_m < 0$  region shows a larger Coulomb effect.

In Figs. 6–9 are shown the same calculations for the  $d_{3/2}$  orbit  $^{40}\text{Ca}$ . Again, we get negligible Coulomb distortion effects with the  $p=q$  and  $\omega-q$  constant kinematics (Fig. 6), some effects with  $p \neq q$  (Figs. 7 and 8), and the largest effect with parallel kinematics. In this particular case, the electron Coulomb distortion enhances the peak for  $p_m < 0$  and reduces the peak for  $p_m > 0$ .

To do the  $2s_{1/2}$  and  $d_{3/2}$  orbit calculations for  $^{40}\text{Ca}$  ( $Z=20$ ), we used 40 electron partial waves and 20 final-state proton partial waves (also 20 virtual photon multipoles). All radial integrals are carried out numerically

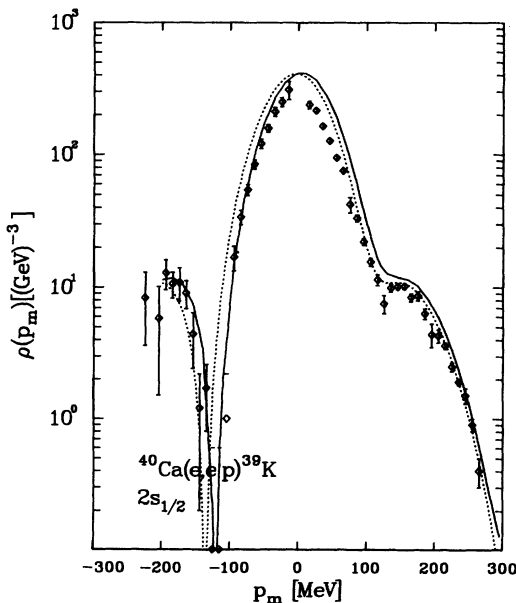


FIG. 5. Reduced cross section for  $^{40}\text{Ca}$  ( $e, e'p$ ) from the  $2s_{1/2}$  shell with parallel kinematics. The kinematics are  $k_0=375$  MeV and  $k'_0=275$ . The solid line is the DWBA calculation, and the dotted line is the PWBA calculation. The data are from Ref. [6].

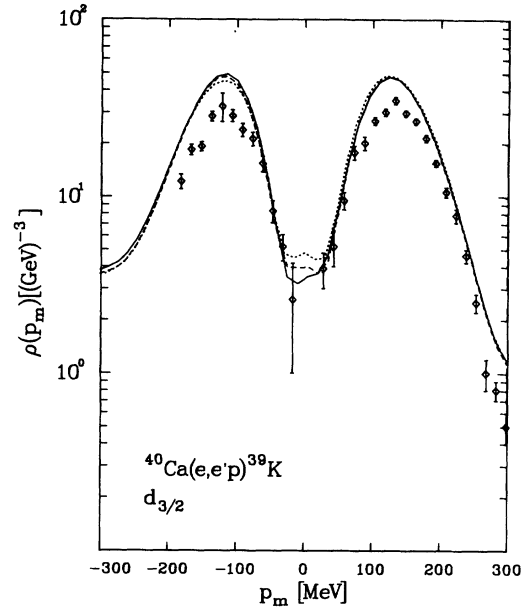


FIG. 6. Reduced cross section for  $^{40}\text{Ca}$  ( $e, e'p$ ) from the  $d_{3/2}$  shell with  $\omega-q$  constant kinematics. The kinematics are  $k_0=375$  MeV,  $k'_0=275$ , and  $p=q$ . The corresponding electron-scattering angle is  $\theta_e=83^\circ$ . The solid line is the DWBA calculation, the dashed line is the DWBA calculation with  $Z=1$ , and the dotted line is the PWBA calculation.

to a radius  $R_{\text{max}}$  well outside the nucleus (determined by the bound-state wave functions), and analytic forms [9] are used to complete the integration to infinity. We work with 14-digit words in the computer and require that all radial integrals be accurate to 6 digits. Even with these precautions, there are a few regions in the cross sections

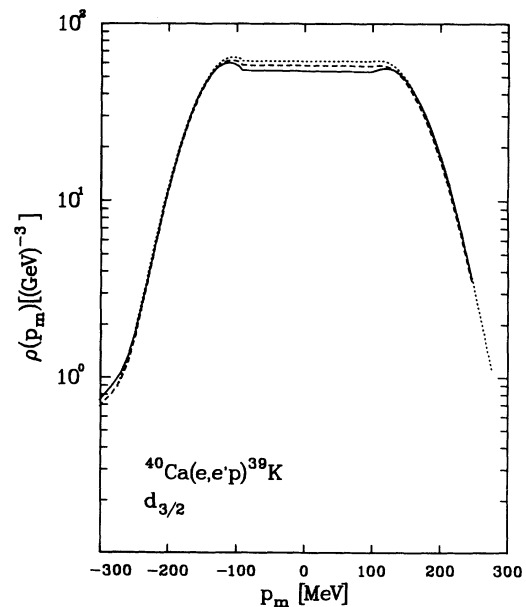


FIG. 7. Reduced cross section for  $^{40}\text{Ca}$  ( $e, e'p$ ) from the  $d_{3/2}$  shell with off-peak  $\omega-q$  constant kinematics. The kinematics are  $k_0=375$  MeV,  $k'_0=265$ , and  $p > q$ ;  $\theta_e=60^\circ$ . The solid line is the DWBA calculation, the dashed line is the DWBA calculation with  $Z=1$ , and the dotted line is the PWBA calculation.

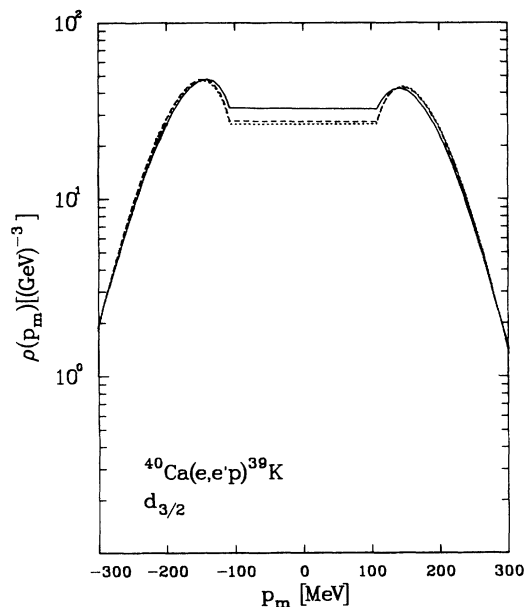


FIG. 8. Reduced cross section for  $^{40}\text{Ca} (e, e'p)$  from the  $d_{3/2}$  shell with off-peak  $\omega$ - $q$  constant kinematics. The kinematics are  $k_0 = 375$  MeV,  $k'_0 = 265$ , and  $p < q$ ;  $\theta_e = 120^\circ$ . The solid line is the DWBA calculation, the dashed line is the DWBA calculation with  $Z = 1$ , and the dotted line is the PWBA calculation.

(minima) where we have found it necessary to take more terms in the expansion to get adequate convergence.

### B. Occupation numbers

If we assume that the shells near the Fermi surface are not completely filled in the shell model, then occupation

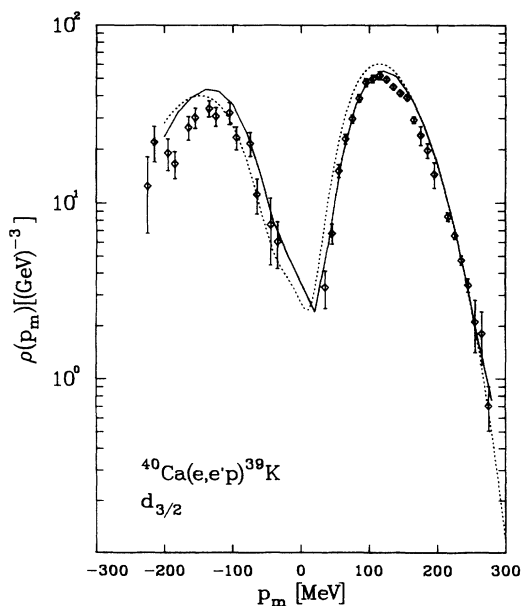


FIG. 9. Reduced cross section for  $^{40}\text{Ca} (e, e'p)$  from the  $d_{3/2}$  shell with parallel kinematics. The kinematics are  $k_0 = 375$  MeV and  $k'_0 = 275$ . The solid line is the DWBA calculation, and the dotted line is the PWBA calculation. The data are from Ref. [6].

numbers will appear as multiplying factors in our calculations. Visual fitting shows that we would need about 75% for the  $2s_{1/2}$  orbital in  $^{40}\text{Ca}$  and 80% for the  $d_{3/2}$  orbital using parallel kinematics data [6]. Occupation numbers, extracted using approximate treatment of the electron distortion [6], are about 50% for the  $2s_{1/2}$  state and about 64% for the  $d_{3/2}$  state; our calculation shows that including the electron distortion properly gives a better fit to the experimental data and more believable occupation numbers. Remember that in our calculation we have no adjustable parameters apart from an overall scaling which is used to determine the occupation probability and all the wave functions we used are predetermined by some other mechanism. We also note that it was observed in Ref. [6] that previous analyses of  $\omega$ - $q$  constant kinematic data tended to find larger occupation numbers than analyses of parallel kinematic data.

## IV. ELECTRON COULOMB DISTORTION EFFECTS FOR LEAD

As we finished the calculation for the  $^{40}\text{Ca}$  cases, a Letter [8] was published by McDermott in which he also presented a DWBA calculation. His calculation used a bound-state wave function from Horowitz and Serot [15] and a relativistic global optical potential to describe the knocked-out proton [11]. The Letter particularly emphasized the calculation for the  $3s_{1/2}$  state in  $^{208}\text{Pb}$ . In the following we attempt to do the same calculation and compare the results.

Besides the relativistic calculations, there is a nonrelativistic calculation which is also used for experimental analysis [7]. This calculation treats the electron distortion in an approximate way by using eikonal-type wave functions to describe the incoming and outgoing electrons. The approximation gives a relatively simple expression compared with the full distorted-wave calculation, but without an exact calculation to verify the accuracy, it is not clear under what conditions the approximation is valid.

In Fig. 10 we compare three calculations: the solid line is the present calculation, the dotted line McDermott's calculation, and the dashed line the nonrelativistic eikonal calculation [7] (the latter two curves are reproduced from Ref. [8]). We first compare the plane-wave approximation calculations; i.e., ignore the electron Coulomb distortion. In doing so we can compare the treatment of the nuclear wave functions: both the bound and free states without the complication of electron distortion. Surprisingly, our results do not agree with McDermott's calculation at all, but agree rather well with the nonrelativistic calculation, especially near the peak. Presumably, the slight differences between our calculation and the nonrelativistic calculation is attributable to differences in the bound-state and continuum wave functions arising from a nonrelativistic versus relativistic approach to describing the nucleus and proton scattering. The disagreement between our results and those of McDermott caused us to spend a lot of time checking the accuracy of our calculation. We checked our code by substituting the code of Horowitz and Serot [15] TIMORA, and

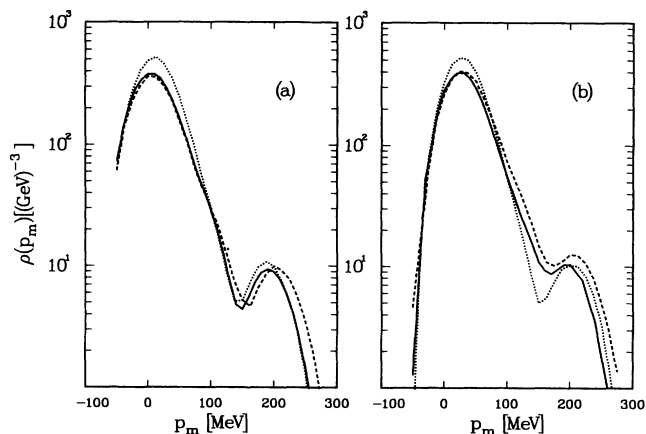


FIG. 10. Reduced cross section for  $^{208}\text{Pb}$  ( $e, e'p$ ) from the  $3s_{1/2}$  shell with parallel kinematics calculated in (a) the PWBA and (b) the DWBA. The solid line is the calculation given in the text, the dashed line is the eikonal calculation from Ref. [7], and the dotted line is McDermott's calculation from Ref. [8].

the code of Hama *et al.* [11], GLOBAL, for our own Hartree and proton-scattering codes. We are also encouraged by our approximate agreement with the nonrelativistic results since we would not anticipate any significant relativistic effects showing up in the ( $e, e'p$ ) cross section at these energies; see also Ref. [16]. We have been unable to discover the basis of our disagreement with McDermott's results.

Next, we examined the Coulomb distortion effects predicted by the three calculations. In our calculation the

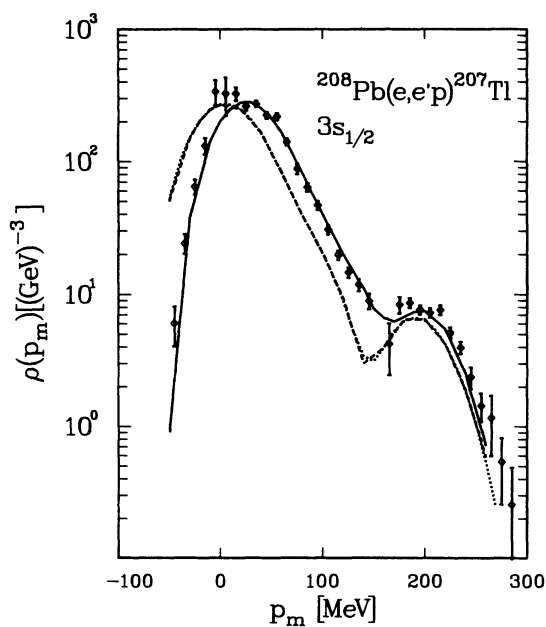


FIG. 11. Reduced cross section for  $^{208}\text{Pb}$  ( $e, e'p$ ) from the  $3s_{1/2}$  shell with parallel kinematics. The kinematics are  $k_0 = 412$  MeV, and proton kinetic energy  $T_p = 100$  MeV. The solid line is the DWBA calculation, the dashed line is the DWBA calculation with  $Z = 1$ , and the dotted line the PWBA calculation. The data are from NIKHEF [17]. The calculated curves are scaled by 0.71.

electron distortion shifts the curve toward higher  $p_m$  with a bigger shift for the first peak than the second peak and partly fills the minimum in between. There is also a slight enhancement of the peak values. The eikonal calculation follows the same general pattern, but the effect is much larger. We roughly agree with McDermott's calculation on the size of the shift of the first peak, but not with the detailed shape changes we find due to Coulomb distortion.

It is interesting to see whether, as in the  $^{40}\text{Ca}$  calculations, we get an occupation number larger than obtained with other calculations. Using an error-weighted least-squares fit to the experimental data [17], the occupation number from our calculation is 1.43 (71.4%). The occupation number obtained using the nonrelativistic eikonal calculations is 1.03 (51.5%), while using McDermott's calculation gives 1.30 (65%). In Fig. 11 we show our best fit to the experimental data.

## V. CONCLUSION

The purpose of this work was to develop an effective way of handling the electron distortion in quasielastic electron scattering. Utilizing the potentials and wave functions of relativistic nuclear physics, the relativistic Hartree calculations, and Dirac phenomenology of the elastic proton scattering, we have developed a code which takes advantage of the supercomputer vectorization capability and properly includes the electron distortions through a partial-wave analysis of the electron wave functions as well as the proton wave functions. The calculation is carried out entirely in relativistic terms, and there is no nonrelativistic reduction involved.

As a preliminary project, we reanalyzed  $^{40}\text{Ca}(e, e'p)$  experimental data using our DWBA code. We examined two orbitals near the Fermi surface of  $^{40}\text{Ca}$ , namely,  $2s_{1/2}$  and  $d_{3/2}$ , with both parallel kinematics and  $\omega$ - $q$  constant kinematics. The calculations show that by properly including the electron distortion, the shapes and minima of the experimental data can be reproduced. We require occupations of 70–80% in order to agree with the experimental data, larger than previous values extracted from ( $e, e'p$ ) cross sections (see Ref. [6]). Using the PWBA result as a reference, Coulomb distortion contributes differently, depending on the kinematics. In  $\omega$ - $q$  constant kinematics, especially if we make the requirement that  $q = p$ , which includes the quasielastic peak condition, Coulomb effects are minimal. But in other cases, Coulomb distortion gives more noticeable effects. In parallel kinematics we find that Coulomb distortion effects cannot be neglected except for the lightest nuclei. The main effects in parallel kinematics are the shifting of the reduced crosssection  $\rho_m$  towards larger  $\rho_m$  and the differential changing of the amplitude as a function of  $\rho_m$ , so that the overall shape of the curve gets changed.

In order to compare with the previous calculation by McDermott [8], we chose the  $3s_{1/2}$  proton in  $^{208}\text{Pb}$  as a subject. Using what we believed to be the same relativistic Hartree bound-state wave function, our calculation does not agree with McDermott's calculation even in the plane-wave limit. Comparing our calculation with the

nonrelativistic calculation of Ref. [7], we find good agreement with the electron distortion turned off and we find that the eikonal method used qualitatively gives the right Coulomb distortion effects, but overestimates them considerably. The occupation number extracted from our calculation is 1.43 (71.4%), which is larger than any previous extracted from  $(e, e'p)$  by using other calculations.

Since it now seems likely that the occupation numbers extracted from  $(e, e'p)$  experiments may agree with those extracted from other reactions and with the theoretical predictions, it is our next project to examine systematically the experimental data available for medium/heavy nuclei.

An item of interest for the future is the separation of the structure functions in the  $(e, e'p)$  process. According to the PWBA, the cross section can be written in terms of

four nuclear structure functions, which could, in principle, be experimentally separated, and many of the experimental arrangements adopted are guided by this prospect. Since our results show that even for  $^{40}\text{Ca}$  the Coulomb effects are noticeable, especially if off-peak kinematics are used, one should be cautious in using plane-wave-based interpretations.

#### ACKNOWLEDGMENTS

We thank the Ohio Supercomputer Center in Columbus for many hours of Cray Y-MP time to develop this calculation and to perform the necessary tests and preliminary projects. This work was supported in part by the U.S. Department of Energy under Grant No. FG02-87ER40370.

- 
- [1] S. Boffi, C. Giusti, F.d. Pacati, and S. Frullani, Nucl. Phys. **A319**, 461 (1979); S. Boffi, C. Giusti, and F.d. Pacati, *ibid.* **A336**, 437 (1980); C. Giusti and F.d. Pacati, *ibid.* **A336**, 427 (1990).
  - [2] W. J. Gerace and A. M. Green, Nucl. Phys. **A93**, 110 (1969).
  - [3] C. Mahaux and R. Sartor, Nucl. Phys. **A484**, 205 (1988).
  - [4] S. M. Banks, B. M. Spicer, G. G. Shute, V. C. Officer, G. J. Wagner, W. E. Dollhopf, Li Qingli, C. W. Glover, D. W. Devins, and D. L. Friesel, Nucl. Phys. **A437**, 381 (1985).
  - [5] N. Matsuoka, M. Fujiwara, H. Sakai, H. Ito, T. Saito, K. Hosono, U. Fujita, and S. Kato, RCNP annual Report, 1985, p. 63.
  - [6] G. J. Kramer, Ph.D. dissertation, University of Amsterdam, 1990.
  - [7] M. Traini, Phys. Lett. **B 213**, 1 (1988); M. Train, S. turck-Chieze, and A. Zghiche, Phys. Rev. **C 38**, 2799 (1988); C. Giusti and F.d. Pacati, Nucl. Phys. **A473**, 717 (1987).
  - [8] J. P. McDermott, Phys. Rev. Lett. **65**, 1991 (1990).
  - [9] L. E. Wright and Indu Talwar, Comput. Phys. Commun. **55**, 367 (1989); Faid Zamani-Noor and D. S. Onley, Phys. Rev. **C 33**, 1354 (1986).
  - [10] Yanhe Jin, Ph.D. dissertation, Ohio University, 1991.
  - [11] S. Hama, B. C. Clark, E. D. Cooper, H. S. Sherif, and R. L. Mercer, Phys. Rev. **C 41**, 2737 (1990).
  - [12] J. M. Eisenberg and W. Greiner, *Excitation Mechanisms of the Nucleus* (North-Holland, New York, 1970).
  - [13] G. Höhler, E. Pietarinen, I. Sabba-Stevescu, F. Borowski, G. G. Simon, V. H. Walther, and R. D. Wendling, Nucl. Phys. **B114**, 505 (1976).
  - [14] T. D. DeForest, Jr., Nucl. Phys. **A392**, 232 (1983).
  - [15] C. J. Horowitz and B. D. Serot, Nucl. Phys. **A368**, 503 (1981).
  - [16] L. Chinitz *et al.*, Phys. Rev. Lett. **67**, 568 (1991).
  - [17] Louk Lapikás (private communication); Edwin Quint, Ph.D. dissertation, University of Amsterdam, 1988.